

# Spatially resolved X-ray absorption spectroscopy investigation of individual cation-intercalated multi-layered $Ti_3C_2T_x$ MXene particles

Ameer Al-Temimy<sup>1,2\*</sup>, Florian Kronast<sup>1</sup>, Mohamad-Assaad Mawass<sup>1</sup>, Katherine A. Mazzio<sup>1</sup>, Kaitlyn Prenger<sup>3</sup>, Michael Naguib<sup>3</sup>, Tristan Petit<sup>1</sup>, and Simone Raoux<sup>1,4\*</sup>

<sup>1</sup> Helmholtz-Zentrum Berlin für Materialien und Energie GmbH, Albert-Einstein-Str. 15, 12489 Berlin, Germany

<sup>2</sup> Department of Physics, Freie Universität Berlin, Arnimallee 14, 14195 Berlin, Germany

<sup>3</sup> Department of Physics and Engineering Physics, Tulane University, New Orleans, LA 70118, USA

<sup>4</sup> Institute of Physics, Humboldt University Berlin, Newtonstr. 15, 12489 Berlin, Germany

Email: [ameer.al-temimy@helmholtz-berlin.de](mailto:ameer.al-temimy@helmholtz-berlin.de), [simone.raoux@helmholtz-berlin.de](mailto:simone.raoux@helmholtz-berlin.de)

Keywords: 2D Materials;  $Ti_3C_2T_x$  MXene; cation intercalation; X-PEEM; X-ray absorption spectroscopy; Individual multi-layered  $Ti_3C_2T_x$  particles

## Abstract:

$Ti_3C_2T_x$  MXene is a two dimensional (2D) material possessing highly active hydrophilic surfaces coupled with high metallic conductivity. Cations intercalation between the  $Ti_3C_2T_x$  nanosheets has a significant role in many applications such as water purification, desalination, and electrochemical energy storage. The pseudocapacitive charging mechanism involving surface redox reactions at the  $Ti_3C_2T_x$  surface enables higher energy densities than electrical double-layer capacitors, and higher power densities than batteries. In this context, the oxidation state of surface Ti atoms involved in redox reactions has a high impact on the capacitance of  $Ti_3C_2T_x$  MXene and this can be impacted by cation intercalation. The electronic structure of multi-layered  $Ti_3C_2T_x$  particles can be investigated by X-ray absorption (XA) spectroscopy, while also benefitting from a high spatial resolution of 30 nm from X-ray photoemission electron microscopy. In this work, the XA spectra from multi-layered intercalated  $Ti_3C_2T_x$  particles of different thicknesses were recorded at the Ti L- and O K-edges. The Ti oxidation state in pristine, Li-, and Mg-intercalated  $Ti_3C_2T_x$  was found to be thickness-dependent, while Na- and K-intercalated  $Ti_3C_2T_x$  particles did not reveal differences upon changing thickness. This work demonstrates thickness dependent modification of the MXene surface chemistry upon cation intercalation in different individual  $Ti_3C_2T_x$  particles.

## Introduction:

The demand for portable electronic devices, electric vehicles, and renewable energy storage devices has increased considerably over the last decade. There is a growing urgent demand for electrochemical energy storage systems where both high energy and high power densities are required simultaneously. The energy density of electrochemical double layer capacitors (EDLCs) is much lower compared to batteries, but they have very high power density (can be charged in seconds). On the other hand, pseudocapacitors can be charged rapidly in a few

minutes or as quickly as less than a minute, achieving power densities exceeding those of batteries [1–4]. In pseudocapacitors, high capacitance is usually achieved due to redox reactions between the electrode and the ion from the electrolyte. There is a wide range of different materials with intrinsic pseudocapacitive behavior such as RuO<sub>2</sub> [5,6], Nb<sub>2</sub>O<sub>5</sub> [2], MnO<sub>2</sub> [7], and VN [8]. However, with the exception of the scarce and costly RuO<sub>2</sub> and VN which would hinder large-scale applications, the poor electrical conductivities limit the high power density capabilities of these materials [5,6,8]. Significant efforts are currently being directed towards developing 2D materials for electrochemical energy storage due to their potentially large electrode-electrolyte interface. For example, reduced graphene oxide [9] enables relatively easy ion insertion between the layers; however, without surface modification with pseudocapacitive active materials, the charge is stored mainly through double layer capacitance.

MXenes are a large family of 2D transition metal carbides, nitrides, and carbonitrides [10,11] that possess superior properties for electromagnetic interference shielding [12], water purification and desalination [13–17], and electrochemical energy storage applications [18–23]. MXenes are synthesized by the selective etching and exfoliation of layered three-dimensional ternary compounds called MAX phases. The MAX phases have a general formula of M<sub>n+1</sub>AX<sub>n</sub> ( $n = 1-3$ ), where M corresponds to an early transition metal, A is typically comprised of elements from groups 13 or 14 of the periodic table, and X is carbon, nitrogen, or a mixture of both [24]. In particular, Ti<sub>3</sub>C<sub>2</sub>T<sub>x</sub> (where T<sub>x</sub> denotes different surface functional groups including –OH, –O–, and –F) can be synthesized by the selective etching of aluminum layers from Ti<sub>3</sub>AlC<sub>2</sub> MAX phase powders, resulting in multi-layered particles with confined water between the Ti<sub>3</sub>C<sub>2</sub>T<sub>x</sub> nanosheets. Previous reports have shown that Ti<sub>3</sub>C<sub>2</sub>T<sub>x</sub> MXene can be intercalated both chemically and electrochemically by organic molecules such as hydrazine, as well as by various of mono- and multivalent cations such as Li<sup>+</sup>, Na<sup>+</sup>, K<sup>+</sup>, and Mg<sup>2+</sup> [21,25–28]. Interestingly, MXenes combine high electrical conductivity with hydrophilic surfaces, enabling fast and reversible insertion of a variety of intercalants in organic and aqueous environments [29–31]. In this contribution, we investigate the impact of cation size (Li<sup>+</sup>, Na<sup>+</sup>, K<sup>+</sup>, Mg<sup>2+</sup>) on the Ti oxidation state of individual MXene particles after intercalation.

Soft X-ray absorption spectroscopy (XAS) [19,32,33] is an element-selective technique that allows investigation of the fine electronic structure of transition metals and is extremely sensitive to surface chemistry. The high chemical sensitivity of XAS at the Ti L-edge has been previously employed to discriminate between various Ti oxide species [34,35]. These oxides can be differentiated because their orbitals differ in their electronic coordination, where TiO, Ti<sub>2</sub>O<sub>3</sub>, and TiO<sub>2</sub> have two, one, and no electrons, respectively [34,35]. X-ray photoemission electron microscopy (X-PEEM) enables acquiring XA spectra with approximately 30 nm spatial resolution under ultra-high vacuum (UHV) conditions [36]. Owing to different chemical bonding environments between surface Ti and O atoms, XAS on pristine and urea-intercalated Ti<sub>3</sub>C<sub>2</sub>T<sub>x</sub> MXene were found to have different signatures [28]. The high chemical sensitivity of XAS can also be employed *in situ* in aqueous environments using flow cells with thin X-ray transparent silicon nitride membranes [28]. Recently we have also demonstrated that cation

intercalation by  $\text{Li}^+$ ,  $\text{Na}^+$ ,  $\text{K}^+$ , and  $\text{Mg}^{2+}$  in  $\text{Ti}_3\text{C}_2\text{T}_x$  MXene can strongly affect the oxidation state of the Ti atoms in MXene after drying in air [37]. Nevertheless, no information about the Ti oxidation state on individual multi-layered particles of these cation-intercalated  $\text{Ti}_3\text{C}_2\text{T}_x$  MXenes have been considered. Furthermore, the influence of different very thin MXene flake sizes on the electrochemical performance in MXene electrodes has been reported [38]. In the latter study, MXene flakes which are only a few layers-thick were used. To avoid confusion with few-layer single flakes, we will refer to individual multi-layered MXene particles in this study, which are comprised of stacked MXene layers having a thickness that can reach several hundreds of nanometers. Because individual MXene particles are the building blocks for multi-layered MXene electrodes, the particle thickness is expected to influence the electrochemical performance of MXene electrodes. In addition, the oxidation state of the Ti atoms in  $\text{Ti}_3\text{C}_2\text{T}_x$  MXene plays an essential role in many applications, in particular for electrochemical energy storage devices. Because MXene-based electrodes are comprised of a wide range of different particle thicknesses, it is necessary to gain insight into how the particle thickness influences the Ti oxidation state.

To do so, the X-PEEM technique was used in this study to characterize pristine, Li-, Na-, K-, and Mg-intercalated  $\text{Ti}_3\text{C}_2\text{T}_x$  MXene using XAS at the Ti L- and O K-edges. X-PEEM enables spatially-resolved XA spectra recorded in partial electron yield (PEY) detection mode over individual particles of multi-layered MXene of different thicknesses. It is worth noting that the probing depth of the PEY detection mode applied in this study is  $\leq 10$  nm. Furthermore, spatially resolved oxidation mapping was used to illustrate the distribution of oxygen content over individual cation-intercalated  $\text{Ti}_3\text{C}_2\text{T}_x$  particles. Two particles with different thicknesses (thin particles are  $\leq 30$  nm while thick ones are  $\geq 200$  nm) were selected for each MXene sample. The Ti oxidation state in pristine, Li-, and Mg- $\text{Ti}_3\text{C}_2\text{T}_x$  was found to be thickness-dependent while Na- and K- $\text{Ti}_3\text{C}_2\text{T}_x$  of different thicknesses did not reveal changes in the Ti oxidation state.

## Results and discussions:

The focus of this study is to investigate the difference in the Ti oxidation state between thick (about 200 to 450 nm) and thin ( $\leq 30$  nm) particles of  $\text{Ti}_3\text{C}_2\text{T}_x$  after intercalation by Li, Na, K, and Mg cations. The thickness of the particles is calculated via multiplying the shadow region length by the tangent of the incident angle ( $16^\circ$ ) of the X-ray beam. **Figure 1a** shows X-PEEM images recorded at the Ti L- and O K-edges of an individual  $\text{Ti}_3\text{C}_2\text{T}_x$  MXene particle. This particle is around two micrometers in diameter,  $\leq 30$  nm thick, and exhibits sharp edges. XA spectra were integrated over regions near the center and edge positions of the particle, the regions of which are highlighted in yellow and green, respectively. The Ti  $L_3$  and  $L_2$  edges are related to the excitation of Ti  $2p_{3/2}$  and Ti  $2p_{1/2}$  core levels to an unoccupied Ti 3d state, respectively, and are each split into two sub peaks. The splitting results from the ligand field induced by binding with oxygen atoms, and corresponds to electronic states with  $t_{2g}$  and  $e_g$  symmetries. Because the Ti  $e_g$  orbitals point directly to the 2p orbitals of the surrounding O atoms, the  $e_g$

band is highly sensitive to changes in the local environment [35,39]. Furthermore, the onset energy position of the Ti L-edge has been found to shift to lower energy with lower Ti oxidation state and vice versa [34].

Changes in the Ti oxidation state of the  $\text{Ti}_3\text{C}_2\text{T}_x$  MXene particle were observed at different locations across its surface. The splitting of the  $L_3$  edge into  $t_{2g}$  (458.1 eV) and  $e_g$  (459.4 eV) sub-bands was observed at the center of the particle but is more pronounced at the edge. **Figure 1b** shows that the onset of the Ti L-edge shifts by +0.4 eV at the edge relative to the center of the particle. However, the lack of clear  $L_2$  edge splitting and a shoulder-like  $e_g$  sub-band suggests an estimated oxidation state higher than  $\text{Ti}^{3+}$  at the center and the edge positions.

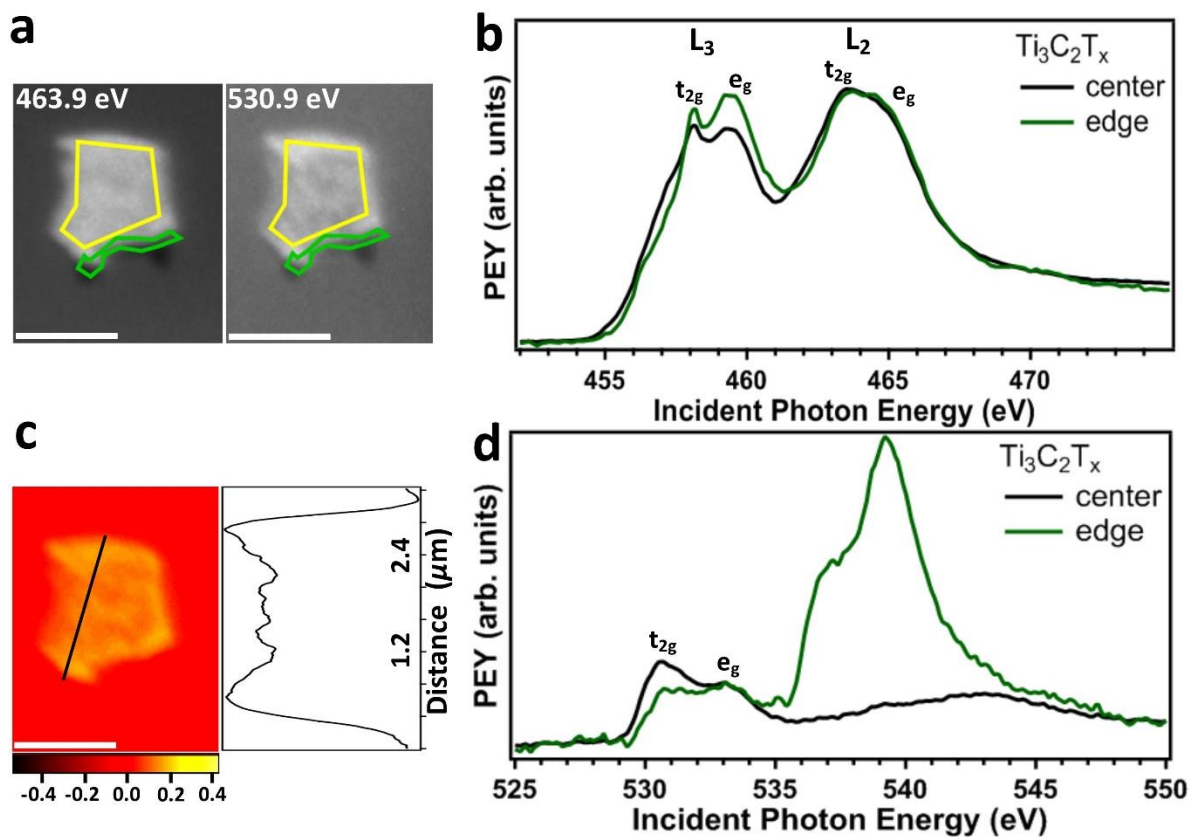


**Figure 1.** (a) X-PEEM micrographs of a pristine multi-layered  $\text{Ti}_3\text{C}_2\text{T}_x$  MXene particle at the Ti L- and O K-edges taken at excitation energies of 463.9 eV and 530.9 eV, respectively (scale bar 2  $\mu\text{m}$ ). The regions labeled center and edge in b and d are highlighted in yellow and green, respectively. (b) X-PEEM Ti L-edge XA spectra of a single particle of pristine  $\text{Ti}_3\text{C}_2\text{T}_x$  MXene. (c) Lateral oxygen concentration over an individual MXene particle obtained from the difference of averaged X-PEEM micrographs at the O K-edge in the  $t_{2g}$  and  $e_g$  region (530.0-534.5 eV) relative to the background (524.5-529.0 eV), the line profile (the y-axis is the intensity in arb. units) of this particle is shown next to the oxygen concentration distribution map. (d) X-PEEM O K-edge XA spectra of pristine  $\text{Ti}_3\text{C}_2\text{T}_x$  MXene.

Since the XA spectra at the Ti L-edge reveal a difference in the Ti oxidation state, the O K-edge was also measured in order to assess any further correlation. **Figure 1c** demonstrates the oxygen distribution and local bonding environment of the  $\text{Ti}_3\text{C}_2\text{T}_x$  MXene particle, where the

relatively higher contrast close to the edges is indicative of a higher oxygen content. The oxygen content within the particle was found to vary slightly but remain lower relative to the edges as illustrated by the line profile in **Figure 1c**. **Figure 1d** shows a comparison in the XA spectra at the O K-edge for pristine  $\text{Ti}_3\text{C}_2\text{T}_x$  MXene at the center and edge positions of the particles. The O K-edge XA spectra demonstrate two main peaks in the energy range between 529.0-535.0 eV which result from the transitions between O 1s and 2p states that are hybridized with empty Ti 3d orbitals. Whereas in the 537.0-546.0 eV region, the O K-edge spectra show a second set of bands which can be attributed to transitions from O 2p states that are hybridized with Ti 4s and 4p states [40]. The strong bands between 537.0-540.0 eV from the edge XAS are characteristic of the  $\text{SiO}_2$  substrate, as demonstrated in **Figure S1**. We will therefore concentrate the discussion on the 529.0-535.0 eV region in the following. The peaks at 530.6 and 533.1 eV are assigned to the  $t_{2g}$  and  $e_g$  sub-bands, respectively. Interestingly, the  $e_g$  peak was found to be higher in intensity compared to the  $t_{2g}$  peak at the edge sites, suggesting a higher oxidation of the edges, which is in agreement with the Ti L-edge. We previously interpreted this result as a slight oxidation induced by oxygen and water molecules from the ambient environment during sample preparation and drying in air [28]. It has to be emphasized that the thickness of the particle shown in Figure 1a is very thin ( $\leq 30$  nm). Nevertheless, the difference in the oxidation state between the center and edge is still represented. Indeed, the oxidation proceeds faster at the edges relative to the basal plane in  $\text{Ti}_3\text{C}_2\text{T}_x$ , resulting in higher resistivity MXene electrodes [41–43]. In comparison to a thicker pristine  $\text{Ti}_3\text{C}_2\text{T}_x$  particle, the total average Ti oxidation state was found to be relatively higher for the thin particle.

The pristine multi-layered  $\text{Ti}_3\text{C}_2\text{T}_x$  MXene particle was presented to probe the impact of the cation intercalation between  $\text{Ti}_3\text{C}_2\text{T}_x$  layers on the Ti oxidation state. Individual Li-intercalated  $\text{Ti}_3\text{C}_2\text{T}_x$  MXene particles were then characterized. **Figure 2a** shows X-PEEM images at the Ti L-edge for two Li- $\text{Ti}_3\text{C}_2\text{T}_x$  particles of different thicknesses. The yellow labeled area indicates the region over which the XA spectra were acquired from, as shown in **Figure 2b**. Thick particles can be identified from the very well pronounced shadow region which is not observed for thin particles. Multi-layered MXene particle 1 XA spectra (about 205 nm thick, **Figure S2**) reveal a very well resolved splitting at the  $L_3$  edge into  $t_{2g}$  (485.1 eV) and  $e_g$  (459.2 eV) peaks. However, no clear splitting was observed in the  $L_2$  edge, resulting in a  $t_{2g}$  peak at 463.4 eV with a shoulder-like  $e_g$  peak. Multi-layered MXene particle 2 is  $\leq 30$  nm thick as no significant shadow is observed (**Figure S2**). This particle shows relatively less pronounced splitting in the  $L_3$  edge into  $t_{2g}$  (457.8 eV) and  $e_g$  (459.2 eV) peaks and the  $L_2$  edge reveals only  $t_{2g}$  (463.1 eV) as no  $e_g$  peak or shoulder-like feature is observed. However, the onset energy position of the Ti L-edge in particle 1 and 2 of Li- $\text{Ti}_3\text{C}_2\text{T}_x$  MXene was found to be unaffected by the thickness difference. In contrast to particle 2, the  $L_3$   $e_g$  peak is higher in intensity relative to the  $L_3$   $t_{2g}$  peak in particle 1. The higher  $L_3$   $e_g$  to  $t_{2g}$  peak intensity ratio and the  $L_2$   $e_g$  shoulder feature in particle 1 suggests a higher Ti oxidation state compared to particle 2.

The lateral oxygen concentration in both particles (**Figure 2c**) demonstrates no change in the

oxygen distribution, as the line profiles of the corresponding particles show a relatively homogenous oxygen content. **Figure 2d** displays the O K-edge spectra of particle 1 and 2 recorded from the same region of interest where the Ti L-edge XA spectra were acquired in **Figure 2a**. The detection of the SiO<sub>2</sub> substrate signature between 537.0 and 540.0 eV at the O K-edge in particle 2 implies a multi-layered MXene particle of probably less than 10 nm thickness. The peaks at 530.5 and 532.6 eV are assigned to the *t*<sub>2g</sub> and *e*<sub>g</sub> orbitals in particle 1, respectively. For particle 2, on the other hand, no clear *e*<sub>g</sub> contribution is detected. This observation is in agreement with the XA spectra at the Ti L-edge which manifests a higher oxidation state in particle 1 relative to particle 2. Interestingly, thinner multi-layered Li-intercalated MXene particle demonstrates less Ti oxidation than the thick one. We therefore conclude that thinner particles are not necessarily more oxidized. Therefore, the Ti L-edge and O K-edge XA spectra present a relatively higher Ti oxidation state in the thick particles. The thickness-dependent Ti oxidation of Li-Ti<sub>3</sub>C<sub>2</sub>T<sub>x</sub> particles is possibly due to a greater intercalation by Li cations between the multi-layered Ti<sub>3</sub>C<sub>2</sub>T<sub>x</sub> MXene nanosheets of thin particles. Regarding the homogeneity of the lateral oxygen concentration, Li cations are known to intercalate very close to the Ti<sub>3</sub>C<sub>2</sub>T<sub>x</sub> surface, suggesting a homogeneous distribution of Li cations which thus serve to effectively shield the Ti atoms at the MXene surface from forming further oxygen bonds [44].

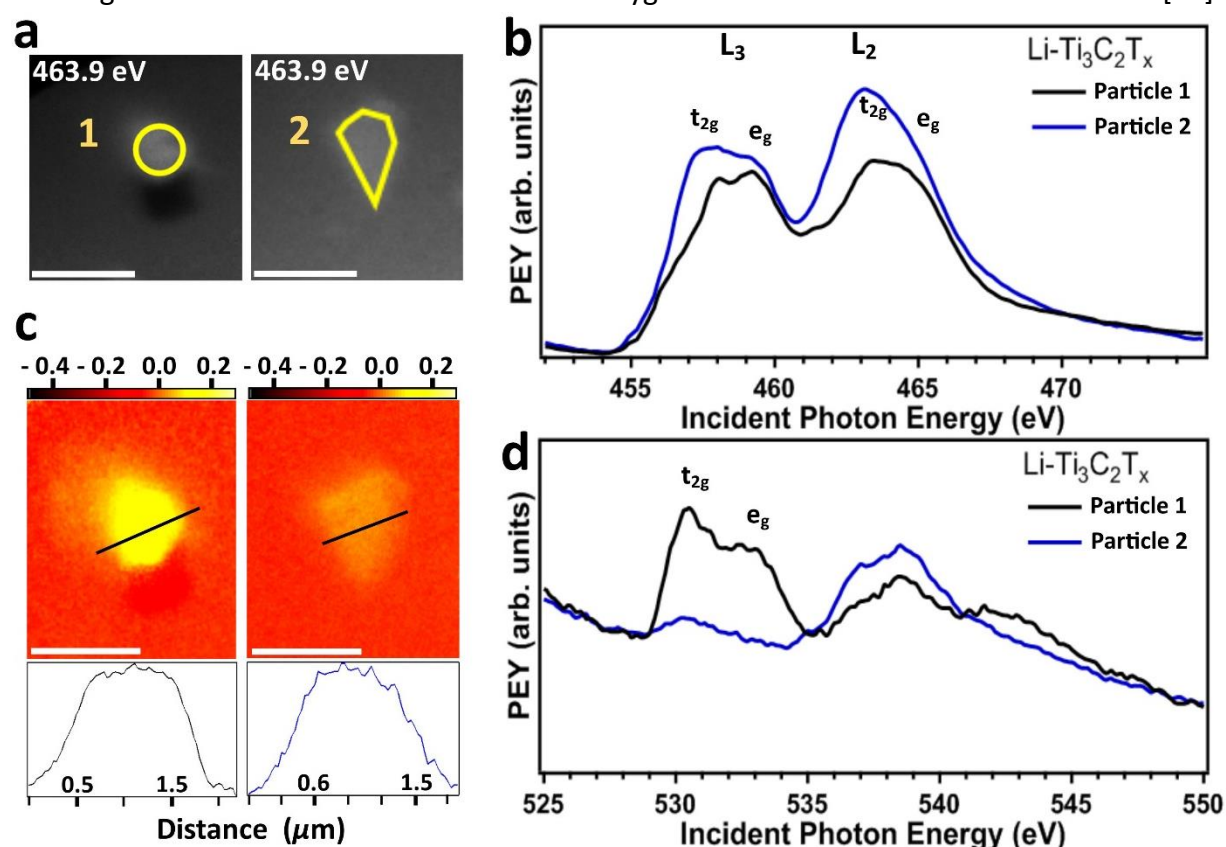


**Figure 2.** (a) X-PEEM micrographs of individual multi-layered Li-Ti<sub>3</sub>C<sub>2</sub>T<sub>x</sub> MXene particles at the Ti L-edge taken at an excitation energy of 463.9 eV (scale bar 2 μm). The investigated region of particle 1 and particle 2 in b and d are labeled in yellow. (b) X-PEEM Ti L-edge XA spectra of the two different Li-Ti<sub>3</sub>C<sub>2</sub>T<sub>x</sub> MXene particles. (c) Lateral oxygen concentration over individual MXene particles obtained for the same energy range described in Figure 1 and the line profile (the y-axis is the intensity in arb. units) across each single particle is shown underneath the oxygen concentration distribution map. (d) X-PEEM O K-edge XA spectra of multi-layeredLi-

### Ti<sub>3</sub>C<sub>2</sub>T<sub>x</sub> MXene particles.

Spatially resolved XA spectra of Na-intercalated multi-layered MXene particles were also measured. The thicknesses of particles 1 and 2 are estimated to be about 270 nm and  $\leq 30$  nm, respectively (**Figure S2**). The X-PEEM micrographs at the Ti L-edge of these two multi-layered MXene particles are shown in **Figure 3a**. Interestingly, both particles reveal faint splitting at the L<sub>3</sub> edge into  $t_{2g}$  (458.0 eV) and  $e_g$  (459.3 eV) peaks while the L<sub>2</sub> edge shows a single peak at 463.5 eV which is related to the  $t_{2g}$  sub-band, as illustrated in **Figure 3b**. In agreement with the Ti L-edge fine structure ( $t_{2g}$  and  $e_g$  peaks), the Ti L-edge onset energy position featured in both Na-Ti<sub>3</sub>C<sub>2</sub>T<sub>x</sub> particles coincide with each other. Irrespective of the thickness of the Na-Ti<sub>3</sub>C<sub>2</sub>T<sub>x</sub> particles, the lateral oxygen concentration map is relatively similar and homogeneous across the particles (**Figure 3c**), which is similar to that observed for Li-Ti<sub>3</sub>C<sub>2</sub>T<sub>x</sub>. The XA spectra at the O K-edge of both multi-layered particles were found to agree with one another (**Figure 3d**). The two O K-edge XA spectra signature are similar, with two distinct peaks at 530.7 eV and 533.3 eV, which are attributed to the  $t_{2g}$  and  $e_g$  orbitals, respectively. This is also observed at the Ti L-edge, and therefore we conclude that there is a comparable oxidation state of the Ti atoms in the two Na-Ti<sub>3</sub>C<sub>2</sub>T<sub>x</sub> MXene particles. As the Ti oxidation state in the multi-layered Na-Ti<sub>3</sub>C<sub>2</sub>T<sub>x</sub> particles is found to be stable irrespective to the particle thickness, the intercalation by Na cations between the multi-layered Ti<sub>3</sub>C<sub>2</sub>T<sub>x</sub> nanosheets might facilitate a relatively homogeneous surface chemistry. It is worth noting that Na cations were also found to prefer sitting close to the Ti<sub>3</sub>C<sub>2</sub>T<sub>x</sub> surface [44].

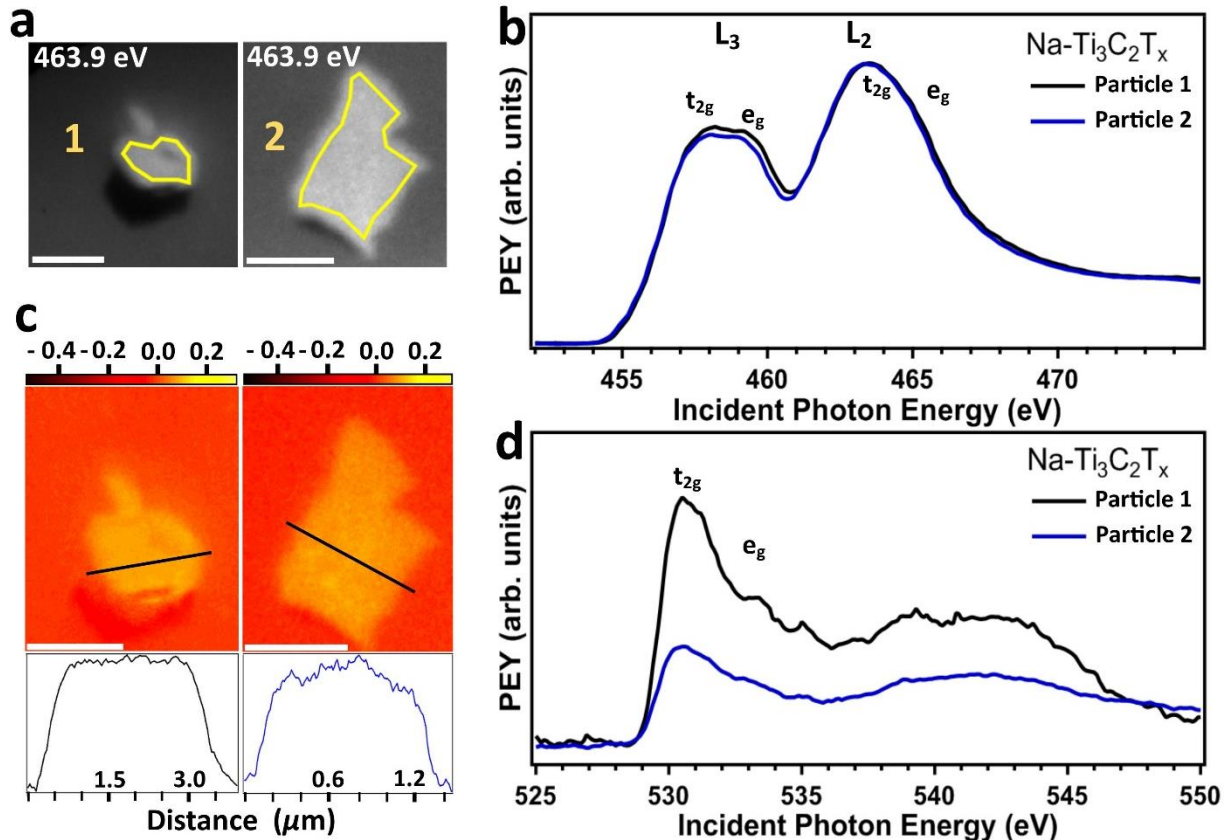


**Figure 3.** (a) X-PEEM micrographs of individual multi-layered Na-Ti<sub>3</sub>C<sub>2</sub>T<sub>x</sub> MXene particles at the Ti L-edge taken at an excitation energy of 463.9 eV (scale bar 3  $\mu\text{m}$  and 1  $\mu\text{m}$  in particle 1 and 2, respectively). The investigated

region of particle 1 and particle 2 in b and d are labeled in yellow. (b) X-PEEM Ti L-edge XA spectra of the two different Na-Ti<sub>3</sub>C<sub>2</sub>T<sub>x</sub> MXene particles. (c) Lateral oxygen concentration over each individual Na-Ti<sub>3</sub>C<sub>2</sub>T<sub>x</sub> particle obtained for the same energy range described in Figure 1 and the line profile (the y-axis is the intensity in arb. units) across each particle is shown underneath the oxygen concentration distribution map. (d) X-PEEM O K-edge XA spectra of multi-layered Na-Ti<sub>3</sub>C<sub>2</sub>T<sub>x</sub> MXene particles.

For K-intercalated Ti<sub>3</sub>C<sub>2</sub>T<sub>x</sub> MXene, two different particles of 450 nm and ≤ 30 nm thick (**Figure S2**) were characterized. The spatially resolved X-PEEM micrographs and the corresponding Ti L-edge XA spectra for the K-Ti<sub>3</sub>C<sub>2</sub>T<sub>x</sub> MXene are presented in **Figure 4a and b**, respectively. Despite the large difference in thickness, the Ti L-edge profile of both multi-layered particles was found to be identical. In both particles 1 and 2, a very weak splitting of the L<sub>3</sub> edge into *t*<sub>2g</sub> (457.8 eV) and *e*<sub>g</sub> (459.0 eV) peaks was observed, while the L<sub>2</sub> edge shows a single peak at 463.4 eV which is related to the *t*<sub>2g</sub> peak, as shown in **Figure 4b**. In line with the Ti L-edge fine structures, the onset energy position in K-Ti<sub>3</sub>C<sub>2</sub>T<sub>x</sub> MXene is found to not be influenced by the thickness of the particles.

However, the lateral oxygen concentration over the particle differs between thick and thin particles. The line profile across the thicker particle demonstrates inhomogeneous oxygen distribution, whereas the thin particle has a relatively homogeneous oxygen distribution as can be seen in **Figure 4c**. The *t*<sub>2g</sub> and *e*<sub>g</sub> peaks of the XA spectra at the O K-edge were found to be at 530.5 eV and 533.2 eV in both particles, respectively (**Figure 4d**). The comparable fine structures at the O K-edge XA profile in both particles leads to a similarity in the Ti oxidation state in multi-layered K-Ti<sub>3</sub>C<sub>2</sub>T<sub>x</sub> MXene particles. This trend observed from O K-edge XA spectra support the similarity in the Ti L-edge XA spectra. Nevertheless, the line profile across the particle reveals differences in the oxygen content environment between thick and thin particles which might be due to the uneven distribution of oxygen atoms in multi-layered Ti<sub>3</sub>C<sub>2</sub>T<sub>x</sub> particles.

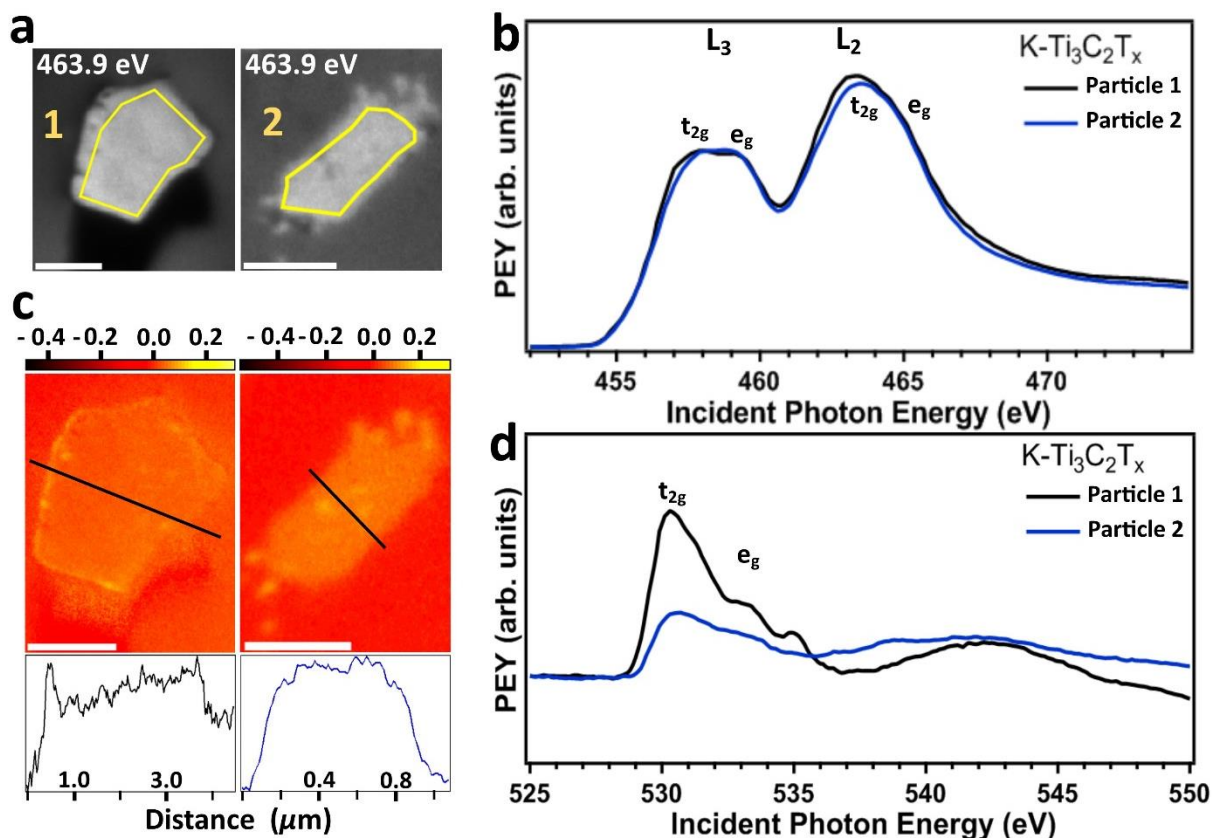


**Figure 4.** (a) X-PEEM micrographs of individual multi-layered K-Ti<sub>3</sub>C<sub>2</sub>T<sub>x</sub> MXene particles at the Ti L-edge taken at an excitation energy of 463.9 eV (scale bar 2 μm and 1 μm in particle 1 and 2, respectively). The investigated region of particle 1 and particle 2 in b and d are labeled in yellow. (b) X-PEEM Ti L-edge XA spectra of the two different K-Ti<sub>3</sub>C<sub>2</sub>T<sub>x</sub> MXene particles. (c) Lateral oxygen concentration over each individual K-Ti<sub>3</sub>C<sub>2</sub>T<sub>x</sub> particle obtained for the same range described in Figure 1 and the line profile (the y-axis is the intensity in arb. units) across each particle is shown underneath the oxygen concentration distribution map. (d) X-PEEM O K-edge XA spectra of multi-layered K-Ti<sub>3</sub>C<sub>2</sub>T<sub>x</sub> MXene particles.

Finally, the impact of intercalation by multivalent cations, such as Mg<sup>2+</sup>, on the surface chemistry in multi-layered Ti<sub>3</sub>C<sub>2</sub>T<sub>x</sub> MXene is of a great interest. The thickness of the investigated Mg-intercalated multi-layered Ti<sub>3</sub>C<sub>2</sub>T<sub>x</sub> particles is about 365 nm and ≤ 30 nm in particles 1 and 2, respectively (see **Figure S2**). **Figure 5a** demonstrates X-PEEM spatially resolved micrographs to show individual particles of Mg-Ti<sub>3</sub>C<sub>2</sub>T<sub>x</sub> MXene at the Ti L-edge. The Ti L-edge XA spectra of both particles demonstrate very similar profiles with a clear splitting in the L<sub>3</sub> edge into *t*<sub>2g</sub> (458.2 eV) and *e*<sub>g</sub> (459.1 eV) peaks, but the L<sub>2</sub> edge shows a single peak at 463.8 eV which corresponds to the *t*<sub>2g</sub> peak, as shown in **Figure 5b**.

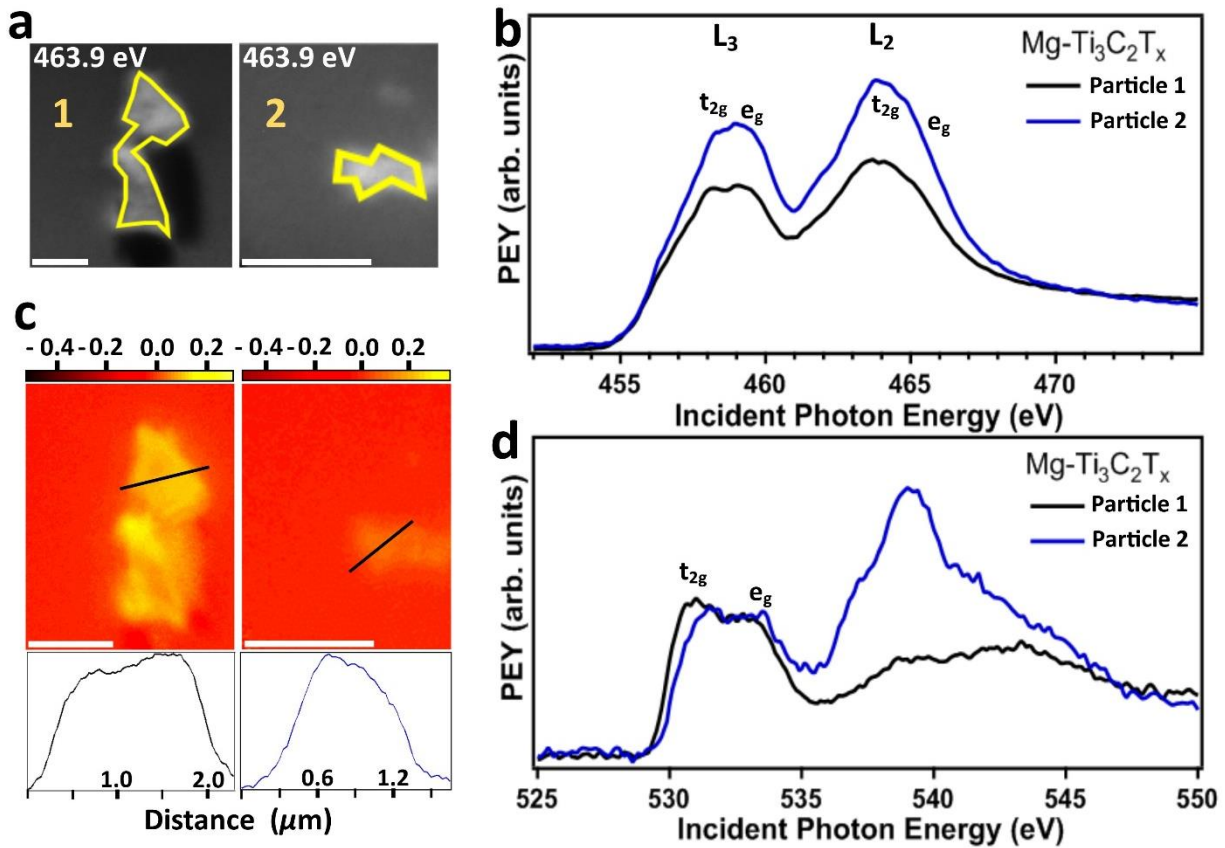


**Figure 5.** (a) X-PEEM micrographs of individual multi-layered Mg-Ti<sub>3</sub>C<sub>2</sub>T<sub>x</sub> MXene particles at the Ti L-edge taken at an excitation energy of 463.9 eV (scale bar 2  $\mu$ m). The investigated region of particle 1 and particle 2 in b and d are labeled in yellow. (b) X-PEEM Ti L-edge XA spectra of the two different Mg-Ti<sub>3</sub>C<sub>2</sub>T<sub>x</sub> MXene particles. (c) Lateral oxygen concentration over each individual Mg-Ti<sub>3</sub>C<sub>2</sub>T<sub>x</sub> particle obtained for the same range described in Figure 1 and the line profile (the y-axis is the intensity in arb. units) across each particle is shown underneath the oxygen concentration distribution map. (d) X-PEEM O K-edge XA spectra of multi-layered Mg-Ti<sub>3</sub>C<sub>2</sub>T<sub>x</sub> MXene particles.

The higher L<sub>3</sub> e<sub>g</sub> to t<sub>2g</sub> peak intensity ratio in particle 2 relative to particle 1 indicates a higher Ti oxidation state. The X-PEEM lateral oxygen concentration map over the entire particles is shown in **Figure 5c**. The line profile across particle 1 and 2, shown below the X-PEEM map, demonstrate an inhomogeneous oxygen distribution. **Figure 5d** shows the XA spectra at the O K-edge of both Mg-Ti<sub>3</sub>C<sub>2</sub>T<sub>x</sub> MXene particles. The t<sub>2g</sub> and e<sub>g</sub> peak position was observed at 531.2 eV (531.6 eV) and 532.9 eV (533.0 eV) in particle 1 (particle 2), respectively. It is worth noting that in the Mg-Ti<sub>3</sub>C<sub>2</sub>T<sub>x</sub> MXene, the distance between the layers are larger after Mg intercalation relative to other cations [45] and Mg cations prefer to be located relatively far away from the MXene surface [46], which paves the way for more oxygen and water molecules from the environment to bond with the Ti<sub>3</sub>C<sub>2</sub>T<sub>x</sub> surface prior sample's introduction to the UHV system. As a result, a higher average Ti oxidation state is observed, as supported by the better resolved splitting observed in the L<sub>3</sub> edge.

In comparison between the different cation-intercalated Ti<sub>3</sub>C<sub>2</sub>T<sub>x</sub> samples, the splitting at the L<sub>3</sub> edge is very well pronounced in Li- and Mg-Ti<sub>3</sub>C<sub>2</sub>T<sub>x</sub> which indicates a higher Ti oxidation

state compared to Na- and K-Ti<sub>3</sub>C<sub>2</sub>T<sub>x</sub> particles. In this context, the multi-layered Na- and K-Ti<sub>3</sub>C<sub>2</sub>T<sub>x</sub> MXene particles demonstrate also lower  $e_g$  to  $t_{2g}$  peak ratio at the O K-edge, which can probably be attributed to a comparable impact induced by these cations on the surface chemistry of the Ti<sub>3</sub>C<sub>2</sub>T<sub>x</sub> MXene. In another recent study, XAS recorded in total electron yield (TEY) mode showed an increase of the Ti oxidation state after intercalation of cations with increasing cation sizes [37]. We observe here a slight difference of the Ti oxidation state after intercalation of Na and K cations. This difference is most likely related to (i) the relatively larger probing depth of TEY relative to PEY detection modes, (ii) the large amount of particles of different size, geometry, and thickness probed by TEY with a larger X-ray spot and (iii) the MXene environment under UHV conditions in this work ( $10^{-9}$  mbar range) compared to standard vacuum ( $10^{-6}$  mbar range) conditions in reference 37. The difference in the pressure, along with the comparison between a thick drop cast sample compared to individual particles, may potentially influence the amount of the confined water between the nanosheets of the multi-layered Ti<sub>3</sub>C<sub>2</sub>T<sub>x</sub> MXene and hence the Ti oxidation state. Furthermore, the oxygen distribution over individual particles in the Li- and Na-Ti<sub>3</sub>C<sub>2</sub>T<sub>x</sub> particles is found to be homogeneous, possibly owing to the preferred position of Li and Na cations close to the Ti<sub>3</sub>C<sub>2</sub>T<sub>x</sub> surface [44]. Note that we previously observed O-Na and O-Li bonds at the O K-edge but not on the individual particles investigated in this study. Further X-PEEM studies would be required to understand where these bonds can be found. In K- and Mg-Ti<sub>3</sub>C<sub>2</sub>T<sub>x</sub> MXene, uneven distribution of oxygen was observed, which would also require further investigation in future.

## Conclusion

By using X-PEEM, the impact of intercalation with Li<sup>+</sup>, Na<sup>+</sup>, K<sup>+</sup>, and Mg<sup>2+</sup> on the electronic structure of individual multi-layered Ti<sub>3</sub>C<sub>2</sub>T<sub>x</sub> MXene particles was investigated. Spatially-resolved XA spectra at the Ti L- and O K-edges provide extensive information about the Ti and O bonding environment over individual multi-layered MXene particles with approximately 30 nm resolution. For each cation-intercalated multi-layered Ti<sub>3</sub>C<sub>2</sub>T<sub>x</sub> MXene, two individual particles of different thickness and lateral dimensions were characterized. The Ti oxidation state in Na- and K-Ti<sub>3</sub>C<sub>2</sub>T<sub>x</sub> MXene was found to be unaffected by the particle thickness, whereas in Li- and Mg-Ti<sub>3</sub>C<sub>2</sub>T<sub>x</sub> MXene, the Ti oxidation state was found to differ between thin and thick particles. This study highlights that the thickness of individual multi-layered MXene particles, in addition to the interlayer spacing, affect the oxidation state of Ti and surface chemistry of MXene which are critical for electrochemical energy storage. This has to be considered to explain their electrochemical performance of thick electrodes based on such cation-intercalated Ti<sub>3</sub>C<sub>2</sub>T<sub>x</sub> MXene multi-layered particles. The X-PEEM-based XA spectra sensitivity at the Ti L- and O K-edges to the oxidation state of the Ti atoms in MXene can also be applied to investigate the intercalation of other cations in Ti<sub>3</sub>C<sub>2</sub>T<sub>x</sub> and/or other types of MXenes.

## Experimental Section:

**Materials:** The  $Ti_3AlC_2$  was synthesized as reported by Huang and Mochalin [47]. Powders of titanium (Ti, Alfa Aesar, -325 mesh), aluminum (Al, Alfa Aesar -325 mesh), and graphite (C, Alfa Aesar, APS 7-15 micron) with Ti : Al : C atomic ratio of 3.00:1.10:1.88, were mixed using a Turbula T2F mixer for 3 h with the aid of yttrium stabilized zirconia balls as mixing medium. Then, the mixed powders were transferred in an alumina crucible and heated in a tube furnace to 1600 °C at 10 °C/minute and held at that temperature for 2 h. Afterward, it was allowed to cool down freely in the furnace to room temperature. Continuous flow of argon was maintained during the entire heating and cooling cycle.

To make pristine  $Ti_3C_2T_x$ , 1 g of  $Ti_3AlC_2$  (-325 mesh) powder was added into 10 mL of 10% hydrofluoric acid (50%, Fisher Scientific) solution. The solution was stirred for 24 h at room temperature. Then, the mixture was centrifuged to remove the acid and fresh deionized water was added, followed by centrifugation, decantation and repeating this cycle until the pH of the suspension reached ~6. After the final centrifugation, fresh DI water was added to collect the sediment that was then dried via vacuum-assisted filtration. The obtained  $Ti_3C_2T_x$  powder was kept under vacuum at room temperature to prevent any deterioration due to oxidation.

Cation-intercalated  $Ti_3C_2T_x$  samples were synthesized following Ghidui et al. [45] procedure.  $Ti_3AlC_2$  (-325 mesh) was slowly added to a solution of lithium chloride in hydrofluoric acid (10% HF) in ratios of 1 g of  $Ti_3AlC_2$  to 10 ml of etchant, with a LiCl :  $Ti_3AlC_2$  molar ratio of 5:1, and stirred for 24 h at room temperature. This was followed by washing with excess deionized water until a pH >6 was reached. The still wet powders were soaked in 37% HCl (30mL per 1 g of powder), centrifuged, and supernatant was discarded. This step was repeated for a total of 5 cycles of acid washing. The powders were again washed with excess deionized water until a pH > 6 was reached. The wet powders were divided into 5 equal portions, and one portion was soaked in 1M LiCl, 1M NaCl, 1M KCl, 0.5M  $MgCl_2$ , or deionized water (40 mL solution for each gram of powder) for 1 h, after which the solutions were centrifuged, and supernatants discarded. This was followed by repeating the soaking of the wet powders in fresh solutions, listed above, for 24 h. Then, the mixtures were washed with deionized water 3 times, discarding supernatants at each step. Finally, the intercalated powders of Li-, Na-, K-, and Mg- $Ti_3C_2T_x$  MXene were dried by vacuum assisted filtration.

All post-synthesis sample preparation and thin film processing for synchrotron-based measurements were carried out in the chemistry lab at the Energy Materials *In situ* Laboratory Berlin (EMIL), jointly operated by Helmholtz-Zentrum Berlin für Materialien and Energie, GmbH (HZB) and the Max-Planck Society. The pristine and cation-intercalated  $Ti_3C_2T_x$  powder samples were dispersed in deionized water (Milli-Q, 18.2 MΩ.cm) (concentration of each sample was 10 mg/ml) and then sonicated for 90 minutes followed by centrifuging at 3500 rpm for 15 minutes. Before use, the samples were sonicated for several minutes in order to obtain a homogeneous suspension (ink-like). Subsequently, to obtain individual and isolated multi-layered particles of MXene, the different MXene samples were spin coated in air on conductive Si substrates.

**X-PEEM:** Photoemission electron microscopy (PEEM) was conducted at the soft X-ray undulator beamline UE49-PGM-A of the BESSY-II storage ring in Berlin using linearly polarized light. The endstation was equipped with an Elmitec PEEM-III energy microscope/analyzer allowing energy and spatially resolved imaging. The XA spectra were measured in Partial Electron Yield (PEY) detection mode under ultra-high vacuum (UHV) conditions. Due to the difficulty to find very close particles in thickness, we focused the study on two individual particles having comparable thickness per each sample. It is worth noting that, X-PEEM technique could also provide valuable information about the thickness of the multi-layered MXene particles. The height of the thick multi-layered MXene particles above the substrate can be measured by their shadow. Please note that the thickness of the multi-layered MXene particles is calculated via multiplying the length of the shadow region by the tangent of the incident angle ( $16^\circ$ ) of the X-ray beam. On the other hand, particles without shadow are below 30 nm of thickness and those particles shining a signal from the substrate are below 10 nm.

## Acknowledgement

A.A. acknowledges the German Academic Exchange Service (DAAD) for financial support during the PhD. A.A. and T.P. acknowledge the financial support from the Volkswagen Foundation (Freigeist Fellowship No. 89592). MAX and MXenes synthesis and characterization at Tulane University was supported as part of the Fluid Interface Reactions, Structures and Transport (FIRST) Center, an Energy Frontier Research Center funded by the U.S. Department of Energy, Office of Science, Office of Basic Energy Sciences. We acknowledge Dr. Babak Anasori for support with some of the sample preparation. The authors acknowledge the kind support by staff members of the BESSY II synchrotron facility. *We thank HZB for the allocation of synchrotron radiation beamtime.*

## Author contributions

The manuscript was written by A.A. with contributions from all coauthors. A.A. designed and conducted the XPEEM study with experimental support from F.K, M.A.M, K.A.M., and S.R. A.A. performed the entire XAS data analysis. M.N. and K.P. conducted the material synthesis. M.N. T.P. and S.R. supervised the research.

## References:

- [1] P. Simon, Y. Gogotsi, Materials for electrochemical capacitors., *Nat. Mater.* 7 (2008) 845–54.
- [2] V. Augustyn, J. Come, M.A. Lowe, J.W. Kim, P.L. Taberna, S.H. Tolbert, H.D. Abruña, P. Simon, B. Dunn, High-rate electrochemical energy storage through Li + intercalation pseudocapacitance, *Nat. Mater.* 12 (2013) 518–522.
- [3] Y. Gogotsi, P. Simon, True performance metrics in electrochemical energy storage, *Science* (80-. ). 334 (2011) 917–918.
- [4] V. Augustyn, P. Simon, B. Dunn, Pseudocapacitive oxide materials for high-rate electrochemical energy storage, *Energy Environ. Sci.* 7 (2014) 1597–1614.
- [5] C.C. Hu, K.H. Chang, M.C. Lin, Y.T. Wu, Design and tailoring of the nanotubular arrayed architecture of hydrous RuO<sub>2</sub> for next generation supercapacitors, *Nano Lett.* 6 (2006) 2690–2695.
- [6] C. Sassoie, C. Laberty, H. Le Khanh, S. Cassaignon, C. Boissière, M. Antonietti, C. Sanchez, Block-copolymer-templated synthesis of electroactive ruo<sub>2</sub>-based mesoporous thin films, *Adv. Funct. Mater.* 19 (2009) 1922–1929.
- [7] M. Toupin, T. Brousse, D. Bélanger, Charge storage mechanism of MnO<sub>2</sub> electrode used in aqueous electrochemical capacitor, *Chem. Mater.* 16 (2004) 3184–3190.
- [8] D. Choi, G.E. Blomgren, P.N. Kumta, Fast and reversible surface redox reaction in nanocrystalline vanadium nitride supercapacitors, *Adv. Mater.* 18 (2006) 1178–1182.
- [9] Z. Tan, G. Chen, Y. Zhu, Carbon-Based Supercapacitors Produced by the Activation of Graphene, *Nanocarbons Adv. Energy Storage.* 1 (2015) 211–225.
- [10] M. Naguib, M. Kurtoglu, V. Presser, J. Lu, J. Niu, M. Heon, L. Hultman, Y. Gogotsi, M.W. Barsoum, Two-dimensional nanocrystals produced by exfoliation of Ti<sub>3</sub>AlC<sub>2</sub>, *Adv. Mater.* 23 (2011) 4248–4253. <https://doi.org/10.1002/adma.201102306>.
- [11] M. Naguib, V.N. Mochalin, M.W. Barsoum, Y. Gogotsi, 25th anniversary article: MXenes: A new family of two-dimensional materials, *Adv. Mater.* 26 (2014) 992–1005. <https://doi.org/10.1002/adma.201304138>.
- [12] F. Shahzad, M. Alhabeb, C.B. Hatter, B. Anasori, S.M. Hong, C.M. Koo, Y. Gogotsi, Electromagnetic interference shielding with 2D transition metal carbides (MXenes), *Science* (80-. ). 353 (2016) 1137–1140.
- [13] J. Wang, P. Chen, B. Shi, W. Guo, M. Jaroniec, S.Z. Qiao, A Regularly Channeled Lamellar Membrane for Unparalleled Water and Organics Permeation, *Angew. Chemie - Int. Ed.* 57 (2018) 6814–6818.
- [14] S. Hong, F. Ming, Y. Shi, R. Li, I.S. Kim, C.Y. Tang, H.N. Alshareef, P. Wang, Two-Dimensional Ti<sub>3</sub>C<sub>2</sub>T<sub>x</sub> MXene Membranes as Nanofluidic Osmotic Power Generators, *ACS Nano.* 13 (2019) 8917–8925.
- [15] L. Ding, Y. Wei, Y. Wang, H. Chen, J. Caro, H. Wang, A Two-Dimensional Lamellar Membrane: MXene Nanosheet Stacks, *Angew. Chemie - Int. Ed.* 56 (2017) 1825–1829.

- [16] K.M. Kang, D.W. Kim, C.E. Ren, K.M. Cho, S.J. Kim, J.H. Choi, Y.T. Nam, Y. Gogotsi, H.T. Jung, Selective Molecular Separation on Ti<sub>3</sub>C<sub>2</sub>T<sub>x</sub>-Graphene Oxide Membranes during Pressure-Driven Filtration: Comparison with Graphene Oxide and MXenes, *ACS Appl. Mater. Interfaces*. 9 (2017) 44687–44694.
- [17] C.E. Ren, K.B. Hatzell, M. Alhabeab, Z. Ling, K.A. Mahmoud, Y. Gogotsi, Charge- and Size-Selective Ion Sieving Through Ti<sub>3</sub>C<sub>2</sub>T<sub>x</sub> MXene Membranes, *J. Phys. Chem. Lett.* 6 (2015) 4026–4031.
- [18] B. Anasori, M.R. Lukatskaya, Y. Gogotsi, 2D metal carbides and nitrides (MXenes) for energy storage, *Nat. Rev. Mater.* 2 (2017) 16098.
- [19] M.R. Lukatskaya, S.M. Bak, X. Yu, X.Q. Yang, M.W. Barsoum, Y. Gogotsi, Probing the Mechanism of High Capacitance in 2D Titanium Carbide Using in Situ X-Ray Absorption Spectroscopy, *Adv. Energy Mater.* 5 (2015) 1500589.
- [20] Y. Xie, M. Naguib, V.N. Mochalin, M.W. Barsoum, Y. Gogotsi, X. Yu, K.W. Nam, X.Q. Yang, A.I. Kolesnikov, P.R.C. Kent, Role of surface structure on li-ion energy storage capacity of two-dimensional transition-metal carbides, *J. Am. Chem. Soc.* 136 (2014) 6385–6394.
- [21] M.R. Lukatskaya, O. Mashtalir, C.E. Ren, Y. Dall’Agnese, P. Rozier, P.L. Taberna, M. Naguib, P. Simon, M.W. Barsoum, Y. Gogotsi, Cation intercalation and high volumetric capacitance of two-dimensional titanium carbide, *Science* (80-. ). 341 (2013) 1502–1505.
- [22] C. Eames, M.S. Islam, Ion intercalation into two-dimensional transition-metal carbides: Global screening for new high-capacity battery materials, *J. Am. Chem. Soc.* 136 (2014) 16270–16276.
- [23] M. Naguib, J. Come, B. Dyatkin, V. Presser, P.L. Taberna, P. Simon, M.W. Barsoum, Y. Gogotsi, MXene: A promising transition metal carbide anode for lithium-ion batteries, *Electrochem. Commun.* 16 (2012) 61–64.
- [24] M.W. Barsoum, MN+1AXN phases: a new class of solids; thermodynamically stable nanolaminates, *Prog. Solid State Chem.* 28 (2000) 201–281.
- [25] O. Mashtalir, M. Naguib, V.N. Mochalin, Y. Dall’Agnese, M. Heon, M.W. Barsoum, Y. Gogotsi, Intercalation and delamination of layered carbides and carbonitrides, *Nat. Commun.* 4 (2013) 1716.
- [26] O. Mashtalir, M.R. Lukatskaya, M.Q. Zhao, M.W. Barsoum, Y. Gogotsi, Amine-assisted delamination of Nb<sub>2</sub>C MXene for li-ion energy storage devices, *Adv. Mater.* 27 (2015) 3501–3506.
- [27] M. Naguib, R.R. Unocic, B.L. Armstrong, J. Nanda, Large-scale delamination of multi-layers transition metal carbides and carbonitrides “mXenes,” *Dalt. Trans.* 44 (2015) 9353–9358.
- [28] A. Al-Temimy, B. Anasori, K.A. Mazzio, F. Kronast, M. Seredych, N. Kurra, M.-A. Mawass, S. Raoux, Y. Gogotsi, T. Petit, Enhancement of Ti<sub>3</sub>C<sub>2</sub> MXene Pseudocapacitance After Urea Intercalation Studied by Soft X-ray Absorption Spectroscopy, *J. Phys. Chem. C.* (2020) [acs.jpcc.9b11766](https://doi.org/10.1021/acs.jpcc.9b11766).

<https://doi.org/10.1021/acs.jpcc.9b11766>.

- [29] Y. Gao, L. Wang, Z. Li, Y. Zhang, B. Xing, C. Zhang, A. Zhou, Electrochemical performance of Ti<sub>3</sub>C<sub>2</sub> supercapacitors in KOH electrolyte, *J. Adv. Ceram.* 4 (2015) 130–134.
- [30] J. Luo, W. Zhang, H. Yuan, C. Jin, L. Zhang, H. Huang, C. Liang, Y. Xia, J. Zhang, Y. Gan, X. Tao, Pillared Structure Design of MXene with Ultralarge Interlayer Spacing for High-Performance Lithium-Ion Capacitors, *ACS Nano.* 11 (2017) 2459–2469.
- [31] X. Wang, S. Kajiyama, H. Iinuma, E. Hosono, S. Oro, I. Moriguchi, M. Okubo, A. Yamada, Pseudocapacitance of MXene nanosheets for high-power sodium-ion hybrid capacitors, *Nat. Commun.* 6 (2015) 6544.
- [32] S.M. Bak, R. Qiao, W. Yang, S. Lee, X. Yu, B. Anasori, H. Lee, Y. Gogotsi, X.Q. Yang, Na-Ion Intercalation and Charge Storage Mechanism in 2D Vanadium Carbide, *Adv. Energy Mater.* 7 (2017) 1700959.
- [33] Y. Xie, M. Naguib, V.N. Mochalin, M.W. Barsoum, Y. Gogotsi, X. Yu, K.W. Nam, X.Q. Yang, A.I. Kolesnikov, P.R.C. Kent, Role of surface structure on li-ion energy storage capacity of two-dimensional transition-metal carbides, *J. Am. Chem. Soc.* 136 (2014) 6385–6394.
- [34] E. Stoyanov, F. Langenhorst, G. Steinle-Neumann, The effect of valence state and site geometry on Ti L<sub>3,2</sub> and O K electron energy-loss spectra of Ti<sub>x</sub>O<sub>y</sub> phases, *Am. Mineral.* 92 (2007) 577–586.
- [35] S.O. Kucheyev, T. Van Buuren, T.F. Baumann, J.H. Satcher, T.M. Willey, R.W. Meulenberg, T.E. Felter, J.F. Poco, S.A. Gammon, L.J. Terminello, Electronic structure of titania aerogels from soft x-ray absorption spectroscopy, *Phys. Rev. B - Condens. Matter Mater. Phys.* 69 (2004) 245102.
- [36] F. Kronast, S. Valencia Molina, SPEEM: The photoemission microscope at the dedicated microfocus PGM beamline UE49-PGMa at BESSY II, *J. Large-Scale Res. Facil. JLSRF.* 2 (2016) A90.
- [37] A. Al-Temimy, K. Prenger, R.G. Golnak, M. Lounasvuori, M. Naguib, T. Petit, The Impact of Cation Intercalation on the Electronic Structure of Ti<sub>3</sub>C<sub>2</sub>T<sub>x</sub> MXenes in Sulfuric Acid, Submitted (n.d.).
- [38] E. Kayali, A. Vahidmohammadi, J. Orangi, M. Beidaghi, Controlling the Dimensions of 2D MXenes for Ultrahigh-Rate Pseudocapacitive Energy Storage, *ACS Appl. Mater. Interfaces.* 10 (2018) 25949–25954. <https://doi.org/10.1021/acsami.8b07397>.
- [39] M.-Y. Hsu, W.-C. Yang, H. Teng, J. Leu, Microstructure and Composition of TiO<sub>2</sub> Nanotube Arrays Fabricated with HF and NH<sub>4</sub>F Electrolytes and Their Evolution during Annealing, *J. Electrochem. Soc.* 158 (2011) K81.
- [40] F.M.F. De Groot, M. Grioni, J.C. Fuggle, J. Ghijsen, G.A. Sawatzky, H. Petersen, Oxygen 1s X-ray-absorption edges of transition-metal oxides, *Phys. Rev. B.* 40 (1989) 5715–5723.
- [41] R. Lotfi, M. Naguib, D.E. Yilmaz, J. Nanda, A.C.T. Van Duin, A comparative study on the oxidation of two-dimensional Ti<sub>3</sub>C<sub>2</sub> MXene structures in different environments, *J.*

- Mater. Chem. A. 6 (2018) 12733–12743.
- [42] C.J. Zhang, S. Pinilla, N. McEvoy, C.P. Cullen, B. Anasori, E. Long, S.H. Park, A. Seral-Ascaso, A. Shmeliov, D. Krishnan, C. Morant, X. Liu, G.S. Duesberg, Y. Gogotsi, V. Nicolosi, Oxidation Stability of Colloidal Two-Dimensional Titanium Carbides (MXenes), *Chem. Mater.* 29 (2017) 4848–4856.  
<https://doi.org/10.1021/acs.chemmater.7b00745>.
- [43] A. Lipatov, M. Alhabeab, M.R. Lukatskaya, A. Boson, Y. Gogotsi, A. Sinitskii, Effect of Synthesis on Quality, Electronic Properties and Environmental Stability of Individual Monolayer Ti<sub>3</sub>C<sub>2</sub> MXene Flakes, *Adv. Electron. Mater.* 2 (2016).
- [44] N.C. Osti, M. Naguib, K. Ganeshan, Y.K. Shin, A. Ostadhossein, A.C.T. Van Duin, Y. Cheng, L.L. Daemen, Y. Gogotsi, E. Mamontov, A.I. Kolesnikov, Influence of metal ions intercalation on the vibrational dynamics of water confined between MXene layers, *Phys. Rev. Mater.* 1 (2017) 065406.
- [45] M. Ghidui, J. Halim, S. Kota, D. Bish, Y. Gogotsi, M.W. Barsoum, Ion-Exchange and Cation Solvation Reactions in Ti<sub>3</sub>C<sub>2</sub> MXene, *Chem. Mater.* 28 (2016) 3507–3514.
- [46] E.S. Muckley, M. Naguib, H.W. Wang, L. Vlcek, N.C. Osti, R.L. Sacci, X. Sang, R.R. Unocic, Y. Xie, M. Tyagi, E. Mamontov, K.L. Page, P.R.C. Kent, J. Nanda, I.N. Ivanov, Multimodality of Structural, Electrical, and Gravimetric Responses of Intercalated MXenes to Water, *ACS Nano.* 11 (2017) 11118–11126.
- [47] S. Huang, V.N. Mochalin, Hydrolysis of 2D Transition-Metal Carbides (MXenes) in Colloidal Solutions, *Inorg. Chem.* 58 (2019) 1958–1966.  
<https://doi.org/10.1021/acs.inorgchem.8b02890>.